Acta Oceanol. Sin., 2024, Vol. 43, No. 8, P. 58–68
https://doi.org/10.1007/s13131-023-2276-5
http://www.aosocean.com
E-mail: ocean2@hyxb.org.cn

The occurrence phases and enrichment mechanism of rare earth elements in cobalt-rich crusts from Marcus-Wake Seamounts

Jingjing Gao[1, 2*], Jihua Liu[1, 2], Hui Zhang[1, 2], Shijuan Yan[1, 2], Xiangwen Ren[1, 2], Quanshu Yan[1, 2]

[1] Key Laboratory of Marine Geology and Metallogeny, First Institute of Oceanography, Ministry of Natural Resources, Qingdao 266061, China

[2] Laboratory for Marine Geology, Laoshan Laboratory, Qingdao 266237, China

Received 21 July 2023; accepted 16 October 2023

Abstract

To explore the occurrence phases and enrichment mechanism of rare earth elements (REEs) in cobalt-rich crusts, this study analyzes the mineral composition and REE contents of the samples from Marcus-Wake Seamounts by XRD, ICP-OES and ICP-MS. The results show that, (1) the cobalt-rich crusts contain the major crystalline mineral (vernadite), the secondary minerals (quartz, plagioclase and carbonate fluorapatite), and a large amount of amorphous ferric oxyhydroxides (FeOOH). (2) The cobalt-rich crusts contains higher Mn (10.83% to 28.76%) and Fe (6.14% to 18.86%) relative to other elements, and are enriched in REEs, with total REE contents of 1 563–3 238 μg/g and Ce contents of 790–1 722 μg/g. Rare earth element contents of the old crusts are higher than those of the new crusts. Moreover, the non-phosphatized crusts have positive Ce and negative Y anomalies, and yet the phosphatized crusts have positive Ce and positive Y anomalies, indicating that cobalt-rich crusts is hydrogenetic and REEs mainly come from seawater. (3) Analytical data also show that the occurrence phases of elements in cobalt-rich crusts are closely related to their mineral phases. In the non-phosphatized crusts, REEs are adsorbed by colloidal particles into the crusts (about 67% of REEs in the Fe oxide phase, and about 17% of REEs in the Mn oxide phase). In contrast, in the phosphatized crusts (affected by the phosphatization), REEs may combine with phosphate to form rare earth phosphate minerals, and about 64% of REEs are enriched in the residual phase containing carbonate fluorapatite, but correspondingly the influence of Fe and Mn oxide phases on REEs enrichment is greatly reduced. In addition, the oxidizing environment of seawater, high marine productivity, phosphatization, and slow growth rate can promote the REE enrichment. This study provides a reference for the metallogenesis of cobalt-rich crusts in the Pacific.

Key words: cobalt-rich crusts, REEs, occurrence phase, enrichment mechanism, Marcus-Wake Seamounts

Citation: Gao Jingjing, Liu Jihua, Zhang Hui, Yan Shijuan, Ren Xiangwen, Yan Quanshu. 2024. The occurrence phases and enrichment mechanism of rare earth elements in cobalt-rich crusts from Marcus-Wake Seamounts. Acta Oceanologica Sinica, 43(8): 58–68, doi: 10.1007/s13131-023-2276-5

1 Introduction

Cobalt-rich crusts are one of important mineral resources on the ocean floor, which are mainly distributed on the seamounts, ridges and plateaus with water depths of 1 500–4 000 m (Hein et al., 2000, 2013; Halbach et al., 2017; Lusty et al., 2018; Fukami et al., 2022). Cobalt-rich crusts are composed of manganese oxides and iron oxyhydroxides, which have great economic value for some strategic elements such as Co, Ni, Cu, Mo, Te and rare earth elements (REEs) (Hein et al., 2016; Marino et al., 2017; Azami et al., 2018; Josso et al., 2021; Zhou et al., 2022). Meanwhile, cobalt-rich crusts grow at very slow rates of 1–10 mm/Ma, and their growth process spans the entire Cenozoic period (Goto et al., 2017; Nishi et al., 2017; Josso et al., 2020; Konstantinova et al., 2022). Therefore, cobalt-rich crusts have been regarded as the concentrated sedimentary strata, which are the recorders of oceanic and climatic history over the past 60 Ma (Gueguen et al., 2016, 2021; Josso et al., 2019; Charles et al., 2020; Konstantinova et al., 2020).

The major minerals of cobalt-rich crusts are vernadite (δ-MnO_2) and amorphous ferric oxyhydroxide (FeOOH) (Hein and Koschinsky, 2014; Conrad et al., 2017; Zhong et al., 2017; Jiang et al., 2020), and the secondary minerals include quartz, feldspar and carbonate fluorapatite (CFA). Koschinsky et al. (Koschinsky and Halbach, 1995; Koschinsky and Hein, 2003; Koschinsky et al., 2020) divide the mineral phases of cobalt-rich crusts into the following four occurrence phases: L1, adsorbed cations (easily leachable) and carbonate phase; L2, Mn oxide phase (easily reducible); L3, Fe oxyhydroxide phase (moderately reducible); L4, residual phase (hardly soluble) with silicates, crystalline oxides, and CFA. Previous studies suggested that a small quantity of alkali metals and alkaline earth metals are mainly enriched in the adsorbed and carbonate phases, while most other elements are mainly enriched in Fe-Mn oxide phases by means of surface adsorption and coprecipitation (Khanchuk et al., 2015; Mikhailik et al., 2017; Surya et al., 2020). Nath et al. (1994) proposed that the REE enrichment in cobalt-rich crusts is influenced by ferric oxide/hydroxide (FeOOH) and Mn oxide (δ-MnO_2), REEs are first adsorbated by FeOOH and then oxidized by δ-MnO_2. The leach-

Foundation item: The fund of Laoshan Laboratory under contract Nos LSKJ202203602 and LSKJ202204103; the China Ocean Mineral Resource Research and Development Association Research Program under contract No. DY135-C1-1-04; the Taishan Scholarship from Shandong Province.

*Corresponding author, E-mail: gaojingjing8@163.com

ing experiment of cobalt-rich crusts on REEs showed that (Bai et al., 2004), amorphous ferric oxyhydroxide has a strong adsorption capacity for REEs, and is the main occurrence phase of REEs. Xu et al. (2008) reported that about 66.4% of REEs are mainly enriched in the Mn oxide phase, which perhaps is associated with the higher Mn content in its Mn oxide phase. Bau and Koschinsky (2009) found through experiments that in non-phosphatized crusts, about 61.73%–81.63% of REEs are enriched in the Fe oxide phase, only about 14.07%–34.05% of REEs are enriched in the Mn oxide phase. Ren et al. (2011a) proposed that in the new non-phosphatized crusts, REE and Y are mainly enriched in the Mn oxide phase, and yet in the old phosphatized crusts, REE and Y mainly exist as separate mineral phases (independent of carbonate fluorapatite), which may be rare earth phosphate minerals. Mohwinkel et al. (2014) found through selective leaching experiments that the REEs enrichment is mainly influenced by the adsorption of the Fe oxide phase, but the contribution of the Mn oxide phase is relatively small. Recently, Huang et al. (2022) presented some different mechanisms to explain this strong enrichment in the Fe-Mn oxide phases, and the experiment showed that the metal elements enter the crusts by surface complexation, redox reactions, and lattice substitution. Among them, Ce^{3+} in seawater is oxidized to Ce^{4+} and enters the Fe oxide phase as CeO_2 precipitation, but other REEs first form anionic complexes and then enter the Fe oxide phase through adsorption.

As above mentioned, these results reflect the complexity of the enrichment mechanism in cobalt-rich crusts, and the enrichment mechanism of REEs is still unclear, so the cobalt-rich crust samples from Marcus-Wake Seamounts in the Pacific are chosen as the research object. In this study, we analyze the mineral composition and REE contents of the samples, and discuss the source, occurrence phases and enrichment mechanism of REEs. This study provides a reference for the metallogenesis of cobalt-rich crusts in the Pacific.

2 Materials and methods

2.1 *Sample descriptions*

The cobalt-rich crusts samples (No. XD3) are collected from Marcus-Wake Seamounts in the Pacific using the dredge during the DY115-18 expedition of R/V *Dayang Yihao* in 2006. The location of the sample XD3 is 19.794 55°N and 157.315 95°E (Fig. 1), with a water depth of 2 450 m.

The sample XD3 is a tabular crust with obvious three-layer structure, which can be sub-divided into dense layer, loose layer and denser layer from top to bottom, and the bedrock is pyroclastic rock (Fig. 2). Of them, the upper dense layer and the middle loose layer are the new crust, and the lower dense layer is the old crust (Fig. 2). Along the growth profile of the crust, five structural layers are divided from top to bottom, followed by upper dense layer, lower dense layer, loose layer, upper denser layer and lower denser layer, marked as XD3(Ⅰ), XD3(Ⅱ), XD3(Ⅲ), XD3(Ⅳ) and XD3(Ⅴ), respectively. Then, 30 micro layers are further obtained by stratification, with sampling spacing of about 4–6 mm, marked as XD3(1) to XD3(30). The sample descriptions of the structural layers and micro layers are shown in Table 1. After drying the sample, grind it to 200 mesh by an agate mortar and place it in a clean sample bag for later use.

2.2 *Major and trace element analytical methods*

Weigh the sample (50.00 ± 0.50) mg for each sample into the dissolved sample liner, then add 1 mL nitric acid, 1 mL hydrochloric acid and 1 mL hydrofluoric acid into the samples respectively, and then put them in a sealed steel sleeve and heat them in an oven at 190℃ for 48 h. After cooling, put it on an electric heating plate at 150℃and steam it dry, then add 3 mL of 30% (*V*/*V*) hydrochloric acid solution and 0.5 mL of 1 μg/g rhodium internal standard solution, and cover it and put it in a sealed steel sleeve, and heat it in an oven at 150℃ for 8 h. After cooling, use 2% (*V*/*V*) nitric acid solution to fix the volume to 50 g, to be measured. Major elements are determined by ICP-OES (Thermo Fisher, USA, iCAP 7400), and trace elements and REEs are determined by ICP-MS (iCAP RQ, Thermo Fisher, USA) at the Key Laboratory of Marine Geology and Metallogeny, First Institute of Oceanography, Ministry of Natural Resources (MNR). The standard materials GBW07337, GBW07338 and GBW07339 are used to monitor data quality in the analysis process. The relative errors of elements are less than 5%, and the recoveries are between 90% and 105%.

2.3 *Chemical leaching method*

According to the chemical leaching method (Koschinsky and

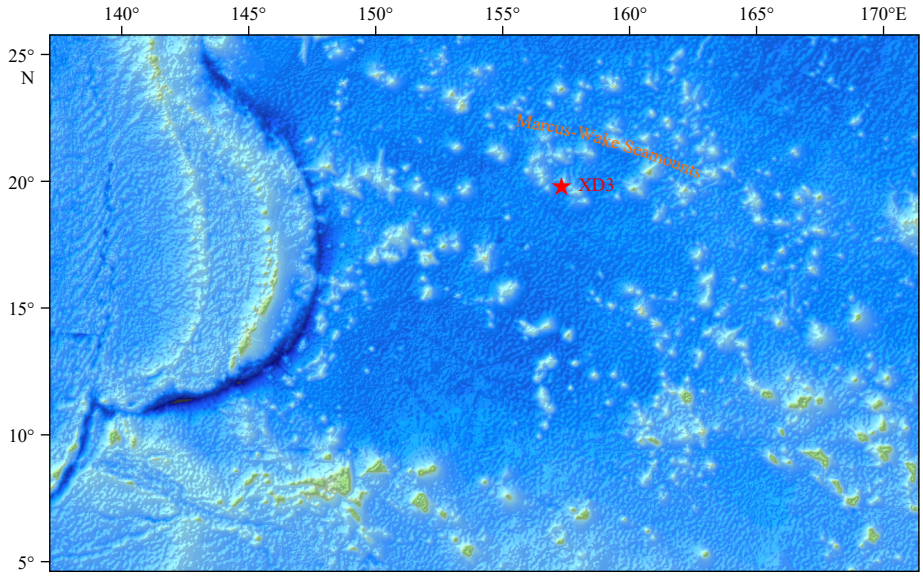

Fig. 1. Location of the cobalt-rich crust XD3.

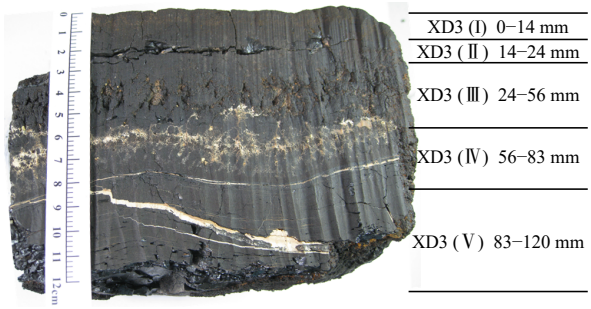

Fig. 2. Photograph of the cobalt-rich crust XD3.

Halbach, 1995; Koschinsky and Hein, 2003), four phases of cobalt-rich crusts are extracted at the Key Laboratory of Marine Geology and Metallogeny, First Institute of Oceanography, MNR, and the experimental steps are as follows.

(1) Exchangeable ions and carbonate phase (referred to as carbonate phase): weigh 1 g of sample, put it in a reaction bottle, add 30 mL of 1 mol/L acetic acid solution (pH = 2.5), and shake at 25℃ for 5 h, after centrifugation of the extract, to be measured.

(2) Mn oxide phase: after washing the residue in step (1), add 175 mL of 0.1 mol/L hydroxylamine hydrochloride solution (pH = 3.7) and shake at 25℃ for 24 h, after centrifugation of the extract, to be measured.

(3) Fe oxide phase: after washing the residue in step (2), add 175 mL of 0.2 mol/L ammonium oxalate solution (pH = 3.5) and shake at 25℃ for 24 h, after centrifugation of the extract, to be measured.

(4) Residual phase: after washing the residue in step (3), transfer to the dissolved sample liner, major elements and trace elements are analyzed according to the Section 2.2. During the experiment, the elements recoveries are between 90% and 105%, and the relative errors are less than 5%. The acetic acid, hydroxylamine hydrochloride, oxalic acid and ammonium oxalate used in the experiment are all superior purity, and the nitric acid, hydrofluoric acid are all obtained by secondary azeotropic distillation, and the water is secondary deionized water.

2.4 *Mineral identification method*

The cobalt-rich crust samples are placed into a special sample carrier cup and pressed into thin slices. X-ray diffractometer (XRD, Nippon Science Corporation, Japan, D/MAX2500HB+/PC) is used for scanning analysis. Studies on mineral identification of samples were performed at the Key Laboratory of Marine Geology and Metallogeny, First Institute of Oceanography, MNR.

3 Results

3.1 *Mineralogical characteristics*

The XRD analytical results of cobalt-rich crusts from Marcus-Wake Seamounts are shown in Fig. 3. The major crystalline mineral is vernadite (δ-MnO_2), which is found in all cobalt-rich crust samples, and many amorphous ferric oxyhydroxides (FeOOH)

Table 1. Description of the cobalt-rich crust XD3

Structural layers number	Micro layers number	Structural layers	Depth/mm	Sample description
XD3(Ⅰ)	XD3(1)	dense layer	0–4	surface oolitic, black brown, dendritic structure
	XD3(2)	dense layer	4–8	black brown, dendritic structure
	XD3(3)	dense layer	8–12	black brown, dendritic structure
	XD3(4)	dense layer	12–14	black brown, dendritic structure
XD3(Ⅱ)	XD3(5)	dense layer	14–19	black brown, columnar structure
	XD3(6)	dense layer	19–24	black brown, columnar structure
XD3(Ⅲ)	XD3(7)	loose layer	24–27	black brown, columnar structure, many clays
	XD3(8)	loose layer	27–30	black brown, columnar structure, many clays
	XD3(9)	loose layer	30–34	black brown, columnar structure, many clays
	XD3(10)	loose layer	34–38	black brown, columnar structure, many clays
	XD3(11)	loose layer	38–42	black brown, columnar structure, many clays
	XD3(12)	loose layer	42–46	black brown, columnar structure, many clays
	XD3(13)	loose layer	46–50	black brown, columnar structure, many clays
	XD3(14)	loose layer	50–54	black brown, columnar structure, many clays
	XD3(15)	loose layer	54–56	black brown, columnar structure, many clays
XD3(Ⅳ)	XD3(16)	denser layer	56–58	Black, columnar structure, some phosphate veins
	XD3(17)	denser layer	58–63	Black, columnar structure, many phosphate veins
	XD3(18)	denser layer	63–67	Black, columnar structure, many phosphate veins
	XD3(19)	denser layer	67–73	Black, columnar structure, some phosphate veins
	XD3(20)	denser layer	73–79	Black, columnar structure, some phosphate veins
	XD3(21)	denser layer	79–83	Black, columnar structure, some phosphate veins
XD3(Ⅴ)	XD3(22)	denser layer	83–89	Bright black, lamellar structure, some phosphate veins
	XD3(23)	denser layer	89–93	Bright black, lamellar structure, some phosphate veins
	XD3(24)	denser layer	93–97	Bright black, lamellar structure, some phosphate veins
	XD3(25)	denser layer	97–101	Bright black, lamellar structure, some phosphate veins
	XD3(26)	denser layer	101–105	Bright black, lamellar structure, some phosphate veins
	XD3(27)	denser layer	105–109	Bright black, lamellar structure, some phosphate veins
	XD3(28)	denser layer	109–113	Bright black, lamellar structure, many phosphate veins
	XD3(29)	denser layer	113–117	Bright black, lamellar structure, many phosphate veins
	XD3(30)	denser layer	117–120	Bright black, lamellar structure, many phosphate veins

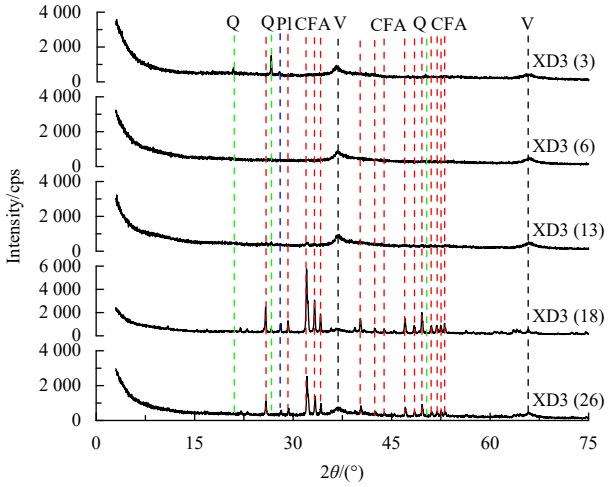

Fig. 3. X-ray diffraction pattern of the cobalt-rich crusts. V-vernadite, Q-quartz, Pl-plagioclase, CFA-carbonate fluorapatite.

are contained in cobalt-rich crusts, as Hein et al. (2000, 2013) suggested. The main detrital minerals of cobalt-rich crusts include quartz and plagioclase. The new crusts XD3(3), XD3(6), and XD3(13) contain more detrital minerals than the old crusts XD3(18) and XD3(26), indicating that cobalt-rich crusts receive more terrigenous detrital materials during forming new crusts (Hein et al., 2000; Conrad et al., 2017). The old crusts XD3(18) and XD3(26) contain more CFA, while the new crusts are almost absent, indicating that cobalt-rich crusts are affected by phosphatization during forming old crusts (Koschinsky et al., 1997; Hein et al., 2016). Therefore, the main mineral phases of cobalt-rich crusts can be sub-divided into Mn mineral phase, Fe mineral phase, detrital mineral phase, and phosphate phase.

3.2 *Major oxides and trace element characteristics*

The major oxides and trace element contents of cobalt-rich crusts from Marcus-Wake Seamounts are shown in Table 2. Of the major elements, Mn and Fe contents are the highest, with Mn ranging from 10.83% to 28.76% and Fe ranging from 6.14% to 18.86%. Next are CaO and P_2O_5, with CaO ranging from 2.87% to 27.74% and P_2O_5 ranging from 0.58% to 16.75%. Then there are Al_2O_3, Na_2O, MgO, TiO_2 and K_2O, with their contents ranging from 0.29% to 2.55%. Again, there are Co, Ni, Ba, Sr, Pb and Cu, with their contents ranging from 0.04% to 0.98%. Finally, there are V, Zn, Mo and Zr, with their contents ranging from 202 μg/g to 1 024 μg/g.

The REE contents of cobalt-rich crusts from Marcus-Wake Seamounts are shown in Table 3. Cobalt-rich crusts are enriched in REE, with REE ranging from 1 563 μg/g to 3 238 μg/g. Among all REEs, Ce content is higher than other elements, with Ce ranging from 790 μg/g to 1 722 μg/g, accounting for about 50% of the total REEs. LREE contents range from 1 271 μg/g to 2 639 μg/g, and HREE contents range from 236 μg/g to 599 μg/g, thus the LREE/HREE ratio is 2.95–5.80, indicating that LREE are higher

Table 2. Major and trace element contents in cobalt-rich crusts

Sample number	Mn/ %	Fe/ %	CaO/ %	P_2O_5/ %	Al_2O_3/ %	Na_2O/ %	K_2O/ %	MgO/ %	TiO_2/ %	Co/ %	Cu/ %	Ni/ %	Ba/ %	Sr/ %	Pb/ %	V/ (μg·g^{-1})	Zn/ (μg·g^{-1})	Zr/ (μg·g^{-1})	Mo/ (μg·g^{-1})
XD3(1)	19.78	18.62	2.96	0.90	1.99	2.34	0.62	1.76	1.55	0.53	0.04	0.28	0.11	0.14	0.17	618	502	577	443
XD3(2)	19.12	18.86	2.87	0.85	1.71	2.31	0.62	1.70	1.61	0.52	0.04	0.28	0.12	0.14	0.16	617	500	620	487
XD3(3)	20.62	18.22	2.92	0.82	1.38	2.23	0.56	1.69	1.63	0.54	0.05	0.32	0.13	0.14	0.17	635	528	597	540
XD3(4)	21.26	17.73	3.07	0.82	1.01	2.29	0.51	1.71	1.62	0.56	0.05	0.35	0.13	0.15	0.18	676	558	530	607
XD3(5)	24.20	15.38	3.34	0.74	0.69	2.30	0.49	1.76	1.86	0.63	0.07	0.43	0.13	0.15	0.18	683	580	412	709
XD3(6)	25.87	13.96	3.50	0.67	0.62	2.27	0.53	1.83	2.09	0.64	0.09	0.53	0.14	0.15	0.18	672	648	412	702
XD3(7)	26.67	13.12	3.48	0.58	0.73	2.32	0.57	1.88	2.12	0.61	0.11	0.61	0.15	0.15	0.17	605	692	493	659
XD3(8)	25.06	13.59	3.42	0.62	0.76	2.24	0.59	1.82	2.12	0.62	0.12	0.55	0.15	0.15	0.16	586	667	534	597
XD3(9)	24.99	13.28	3.39	0.59	0.87	2.24	0.59	1.84	2.00	0.67	0.13	0.54	0.15	0.14	0.15	587	676	550	610
XD3(10)	25.45	12.31	3.69	0.79	1.38	2.32	0.69	2.01	2.05	0.77	0.15	0.62	0.16	0.14	0.13	576	747	548	627
XD3(11)	23.85	11.90	4.28	1.31	1.35	2.19	0.76	2.00	2.17	0.75	0.15	0.60	0.17	0.13	0.13	553	771	577	571
XD3(12)	26.70	11.03	4.43	1.26	1.22	2.28	0.79	2.24	1.92	0.73	0.18	0.80	0.18	0.13	0.12	587	920	559	721
XD3(13)	26.70	10.64	4.59	1.33	1.23	2.38	0.78	2.24	1.77	0.67	0.19	0.83	0.18	0.13	0.12	584	926	540	758
XD3(14)	28.76	11.29	4.52	1.11	0.95	2.55	0.76	2.37	1.63	0.63	0.21	0.98	0.19	0.13	0.13	591	1 024	503	833
XD3(15)	27.29	10.68	5.62	1.84	0.75	2.38	0.70	2.24	1.51	0.58	0.20	0.94	0.18	0.13	0.13	548	974	464	805
XD3(16)	23.46	9.31	10.80	5.20	0.87	2.37	0.65	2.00	1.28	0.42	0.17	0.80	0.16	0.13	0.11	488	830	449	676
XD3(17)	13.97	6.14	26.12	15.49	1.27	1.86	0.56	1.35	0.91	0.20	0.10	0.40	0.10	0.13	0.06	282	456	376	320
XD3(18)	10.83	7.08	27.74	16.75	1.23	1.79	0.56	1.18	0.95	0.15	0.08	0.23	0.10	0.13	0.07	283	364	386	202
XD3(19)	20.92	11.96	12.38	6.08	1.33	2.06	0.62	1.62	1.88	0.39	0.15	0.36	0.21	0.15	0.13	590	615	664	482
XD3(20)	20.96	14.42	10.42	4.93	0.97	2.12	0.48	1.48	2.05	0.38	0.15	0.31	0.25	0.17	0.16	708	640	807	505
XD3(21)	21.26	14.51	15.14	8.20	0.69	1.95	0.56	1.48	1.11	0.35	0.16	0.40	0.19	0.16	0.14	666	598	508	770
XD3(22)	22.73	14.59	9.01	3.95	0.58	1.91	0.46	1.42	1.59	0.34	0.13	0.29	0.25	0.18	0.22	874	671	566	792
XD3(23)	20.79	13.27	12.30	5.85	0.55	1.90	0.45	1.33	1.44	0.30	0.11	0.26	0.24	0.18	0.20	780	609	502	701
XD3(24)	21.62	11.74	13.23	6.47	0.42	1.89	0.46	1.32	1.37	0.29	0.10	0.28	0.22	0.18	0.18	752	569	417	683
XD3(25)	20.42	11.89	13.66	7.24	0.57	1.93	0.43	1.28	1.47	0.26	0.09	0.26	0.23	0.18	0.18	732	560	408	666
XD3(26)	19.84	11.83	15.63	8.12	0.40	1.80	0.41	1.22	1.50	0.22	0.07	0.23	0.23	0.18	0.18	719	556	383	600
XD3(27)	21.22	12.61	11.24	5.40	0.34	1.87	0.43	1.29	1.68	0.26	0.06	0.25	0.26	0.18	0.20	798	618	376	693
XD3(28)	20.92	12.74	11.09	5.24	0.31	1.80	0.43	1.28	1.78	0.26	0.05	0.24	0.28	0.19	0.20	818	639	366	736
XD3(29)	21.50	13.40	11.62	5.55	0.29	1.79	0.42	1.27	1.65	0.27	0.05	0.22	0.30	0.19	0.20	818	642	336	778
XD3(30)	20.62	13.98	12.90	6.65	0.51	1.67	0.38	1.23	1.55	0.26	0.05	0.22	0.31	0.19	0.22	728	606	392	652

Table 3. REE contents in cobalt-rich crusts

Sample number	La/ (μg·g^{-1})	Ce/ (μg·g^{-1})	Pr/ (μg·g^{-1})	Nd/ (μg·g^{-1})	Sm/ (μg·g^{-1})	Eu/ (μg·g^{-1})	Gd/ (μg·g^{-1})	Tb/ (μg·g^{-1})	Dy/ (μg·g^{-1})	Ho/ (μg·g^{-1})	Er/ (μg·g^{-1})	Tm/ (μg·g^{-1})	Yb/ (μg·g^{-1})	Lu/ (μg·g^{-1})	Y/ (μg·g^{-1})	REE/ (μg·g^{-1})	LREE/ (μg·g^{-1})	HREE/ (μg·g^{-1})	LREE/ HREE	δCe	δEu
XD3(1)	288	904	67.23	270	58.14	14.00	64.01	9.69	57.37	11.02	30.39	4.22	27.73	3.95	205	2 015	1 601	414	3.87	1.42	1.01
XD3(2)	303	866	65.55	265	55.74	13.70	61.73	9.48	57.96	11.16	31.08	4.33	28.08	4.09	210	1 987	1 569	418	3.76	1.34	1.03
XD3(3)	323	847	66.61	271	55.74	13.61	62.85	9.66	60.96	11.88	33.19	4.68	30.13	4.40	215	2 009	1 577	432	3.65	1.25	1.01
XD3(4)	328	857	68.00	273	56.10	13.73	63.42	9.72	60.54	11.83	32.89	4.66	30.33	4.34	218	2 033	1 597	436	3.67	1.24	1.01
XD3(5)	328	951	73.97	289	60.84	14.51	65.10	9.91	60.31	11.58	32.38	4.59	29.17	4.26	187	2 121	1 717	404	4.25	1.33	1.01
XD3(6)	290	958	70.88	271	58.22	13.62	60.50	9.10	53.31	9.94	27.44	3.92	25.49	3.63	170	2 025	1 662	363	4.58	1.46	1.01
XD3(7)	239	985	58.75	221	48.26	11.14	50.27	7.39	42.49	7.81	21.57	3.18	20.65	2.95	131	1 850	1 562	288	5.43	1.81	0.99
XD3(8)	227	964	54.58	203	44.18	10.42	48.06	6.76	38.80	7.18	19.94	2.89	19.15	2.70	131	1 781	1 504	277	5.44	1.88	0.99
XD3(9)	198	909	46.48	172	36.95	8.75	41.50	5.69	33.14	6.07	17.01	2.48	16.50	2.34	112	1 608	1 371	236	5.80	2.07	0.98
XD3(10)	200	927	46.29	177	38.18	9.17	44.10	6.15	35.70	6.83	19.15	2.73	17.45	2.53	129	1 660	1 397	263	5.31	2.10	0.98
XD3(11)	222	903	54.76	217	46.61	11.29	52.64	7.57	45.70	8.92	24.63	3.37	20.97	2.97	193	1 815	1 455	360	4.04	1.78	1.00
XD3(12)	229	936	54.13	211	44.89	11.11	51.90	7.49	45.85	9.09	25.04	3.42	21.54	3.11	192	1 845	1 486	360	4.13	1.83	1.01
XD3(13)	223	919	50.36	199	42.13	10.32	50.21	7.14	43.01	8.60	24.28	3.36	21.13	3.02	195	1 799	1 444	355	4.06	1.89	0.99
XD3(14)	219	797	48.50	187	38.40	9.75	44.27	5.86	38.36	6.73	18.17	2.61	16.49	2.43	145	1 579	1 299	280	4.64	1.68	1.04
XD3(15)	218	790	45.12	173	35.46	9.16	42.55	5.59	37.28	6.78	18.89	2.76	17.71	2.65	157	1 563	1 271	292	4.36	1.73	1.04
XD3(16)	228	900	37.90	147	28.32	7.43	38.05	5.08	34.41	8.20	25.55	3.94	26.48	4.16	308	1 803	1 349	453	2.98	2.07	0.99
XD3(17)	228	894	39.07	155	30.50	7.66	38.86	5.45	36.03	8.08	24.62	3.66	24.32	3.90	314	1 812	1 354	459	2.95	2.03	0.98
XD3(18)	249	1 052	49.77	198	38.88	9.61	47.21	6.54	40.03	8.65	24.77	3.44	22.85	3.51	319	2 074	1 598	476	3.35	2.05	0.98
XD3(19)	266	1 170	61.11	241	49.14	11.98	57.34	7.67	43.92	8.51	23.12	3.08	19.09	2.78	212	2 176	1 799	377	4.77	2.00	0.99
XD3(20)	303	1 358	68.21	269	53.74	13.09	65.82	8.53	49.25	9.38	25.38	3.33	21.08	3.00	237	2 488	2 065	423	4.88	2.06	0.97
XD3(21)	296	1 202	54.20	207	39.35	9.66	48.70	6.80	42.21	8.38	24.08	3.51	23.26	3.41	268	2 237	1 809	428	4.22	2.04	0.97
XD3(22)	288	1 234	49.36	183	32.86	8.25	46.44	5.81	33.99	6.63	18.74	2.71	17.70	2.58	256	2 186	1 796	391	4.60	2.22	0.93
XD3(23)	312	1 340	58.77	221	38.74	9.54	54.87	7.14	43.89	9.05	25.70	3.79	24.62	3.62	248	2 400	1 980	420	4.71	2.13	0.91
XD3(24)	266	1 160	52.33	198	34.39	8.76	48.79	6.56	41.48	8.70	25.25	3.70	24.03	3.54	284	2 165	1 720	446	3.86	2.13	0.94
XD3(25)	275	1 197	51.61	192	33.26	8.45	48.34	6.24	38.97	8.09	23.18	3.37	22.06	3.25	245	2 156	1 757	398	4.41	2.17	0.93
XD3(26)	332	1 406	60.49	223	38.00	9.25	53.16	6.66	40.57	8.32	23.80	3.40	22.43	3.30	240	2 471	2 069	402	5.15	2.14	0.90
XD3(27)	353	1 532	65.13	239	40.28	9.70	57.09	6.89	40.76	8.42	24.42	3.45	23.00	3.42	278	2 685	2 239	445	5.03	2.18	0.89
XD3(28)	373	1 662	78.07	290	50.79	12.27	69.67	9.01	54.64	11.60	33.59	4.79	31.09	4.61	276	2 962	2 467	495	4.99	2.11	0.91
XD3(29)	419	1 722	89.34	330	58.02	14.21	77.13	10.34	64.50	12.80	40.10	5.62	36.44	5.32	341	3 225	2 632	593	4.44	1.93	0.93
XD3(30)	424	1 711	89.64	341	59.49	14.60	78.26	10.32	64.41	12.69	39.69	5.60	35.90	5.28	347	3 238	2 639	599	4.41	1.91	0.94

Note: LREE = La + Ce + Pr + Nd + Sm + Eu, HREE = Gd + Tb + Dy + Ho + Er + Tm + Yb + Lu + Y, $\delta Ce = 2Ce_N/(La_N + Pr_N)$, $\delta Eu = 2Eu_N/(Sm_N + Gd_N)$, La_N, Ce_N, Pr_N, Sm_N, Eu_N and Gd_N are normalized by North American shale (NASC), and NASC data are from Wang et al. (1989).

than HREE. The δCe ranges from 1.24 to 2.22, and δCe >1, indicating that the cobalt-rich crusts have positive Ce anomaly. The δEu ranges from 0.89 to 1.04, and δEu ≈ 1, indicating that the cobalt-rich crusts have no obvious Eu anomaly. In addition, the average content of REEs in the upper crust is 2 032 μg/g, and that in the middle crust is 1 722 μg/g, and that in the lower crust is 2 405 μg/g, so REE contents of the old crusts are higher than those of the new crusts.

4 Discussion

4.1 *Origin of cobalt-rich crusts*

Marine ferromanganese deposits can be generally sub-divided into three origins: hydrogenetic, diagenetic and hydrothermal (Halbach, 1986; Liu and Wang, 2021). The metal ions of hydrogenetic ferromanganese deposits come from seawater, and the main components are the Fe-Mn oxides precipitated by colloidal particles in seawater. They are usually formed under strong oxidation condition, and the growth rate is very slow, generally ranging from 1 mm/Ma to 10 mm/Ma. REE contents are above 1 500 μg/g, and REE distribution patterns normalized by North American shale (NASC) show positive Ce and negative Y anomalies (Hein et al., 2013, Bau et al., 2014). The metal ions of diagenetic ferromanganese deposits come from the pore water in the sediment or sediment-water interface under suboxidation condition (Marino et al., 2019). They are usually formed under weak oxidation condition, and REE contents are generally lower than those of diagenetic Fe-Mn deposits, about 1 000 μg/g, and REE distribution patterns normalized by NASC show negative Ce and Y anomalies (Marino et al., 2019). The metal ions of hydrothermal ferromanganese deposits come from the hydrothermal fluids that erupt from the seafloor at medium-low temperature, with the fastest growth rate, and REE contents generally are lower than 100 μg/g. REE distribution patterns normalized by NASC show negative Ce and positive Y anomalies (Pelleter et al., 2017). In this study, REE contents of cobalt-rich crusts are 1 563–3 238 μg/g, δCe > 1 and δY < 1 in the non-phosphatized crusts, indicating positive Ce anomaly and negative Y anomaly, all of which are consistent with hydrogenetic Fe-Mn crusts.

According to the Fe-(Co + Cu + Ni) × 10-Mn ternary diagram (Bonatti et al., 1972) and the (Cu + Ni) × 15- (Zr + Y + Ce) × 100-(Fe + Mn)/4 ternary diagram (Josso et al., 2017), the origin of ferromanganese deposits can be distinguished. The results show that (Fig. 4), the sample points are all plotted within the hydrogenetic area, which indicate that the cobalt-rich crusts are hydrogenetic and are not affected by submarine hydrothermal activity and diagenesis. Meanwhile, according to δCe-Nd and δCe-Y_N/Ho_N correlation diagram (Bau et al., 2014), the origin of ferromanganese deposits can also be distinguished. The results show that (Fig. 5), Nd > 100 μg/g, δCe > 1 and Y_N/Ho_N < 1.5, the sample points are all plotted within the hydrogenetic area, which indicate that the cobalt-rich crusts are hydrogenetic and are not affected by submarine hydrothermal activity and diagenesis.

NASC-normalized REE distribution patterns show that (Fig. 6), the non-phosphatized crusts have positive Ce and negative Y anomalies, while the phosphatized crusts have positive Ce and Y anomalies. The increase of Y content in the phosphatized crusts is caused by the phosphate mixing (Koschinsky et al., 1997; Koschinsky and Hein, 2003; Ren et al., 2016). Seawater shows negative Ce and positive Y anomalies, and REE pattern of the non-phosphatized crusts mirrors that of seawater, indicating that REEs in seawater are consumed during forming cobalt-rich crusts. Therefore, REEs of cobalt-rich crusts mainly come from seawater. In addition, Fe-Mn oxides and marine phosphates are two typical marine authigenic components (Pan et al., 2002, 2005), and their REEs come from seawater. The phosphate rock on seamount has a REE pattern similar to seawater, showing negative Ce and positive Y anomalies, indicating that marine phosphates inherit the REE pattern of seawater. So the unique REE pattern of seawater is the result of the balance between supply and consumption (Ren et al., 2017).

4.2 *Enrichment mechanism of REEs*

In order to reveal the occurrence phases and enrichment mechanism of REEs in cobalt-rich crusts from Marcus-Wake Seamounts, scientists have separated the following four phases (Koschinsky and Halbach, 1995; Koschinsky and Hein, 2003; Gao et al., 2015, 2023): carbonate phase, Mn oxide phase, Fe oxide phase and residual phase. The phase distribution of its elements in structural layers is shown in Fig. 7. In the non-phosphatized crusts XD3(Ⅰ), XD3(Ⅱ), and XD3(Ⅲ), Na, K, Ca, Mg, and Sr are mainly enriched in the carbonate phase, and Mn, Ba, Sr, Co and

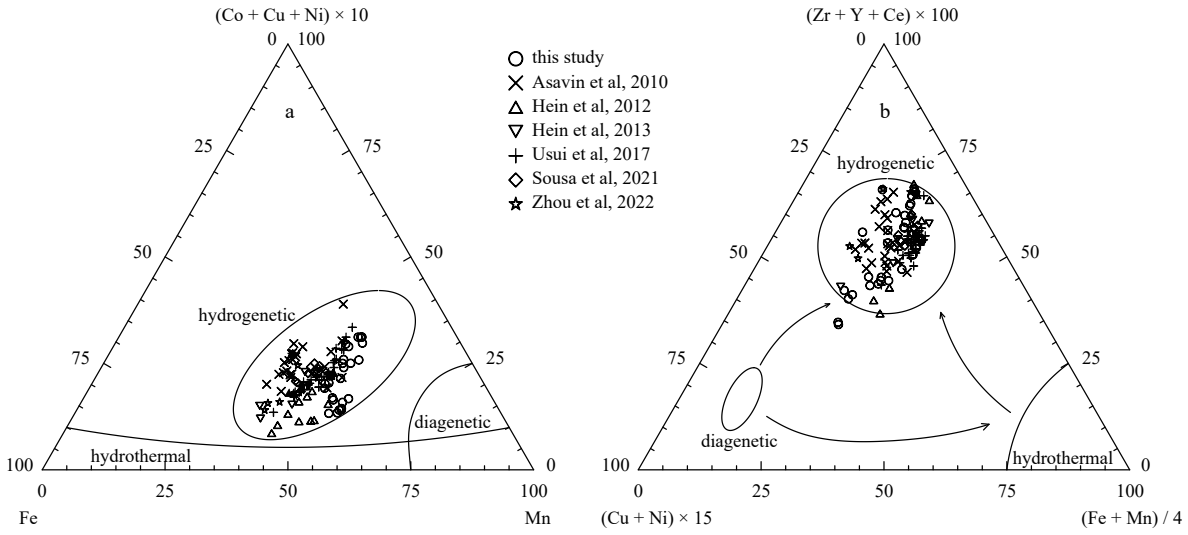

Fig. 4. Ternary diagram in cobalt-rich crusts: a. Fe-(Co + Cu + Ni) × 10-Mn; b. (Cu + Ni) × 5-(Zr + Y + Ce) × 100- (Fe + Mn)/4 (Asavin et al., 2010; Hein et al., 2012, 2013; Usui et al., 2017; Sousa et al., 2021; Zhou et al., 2022)

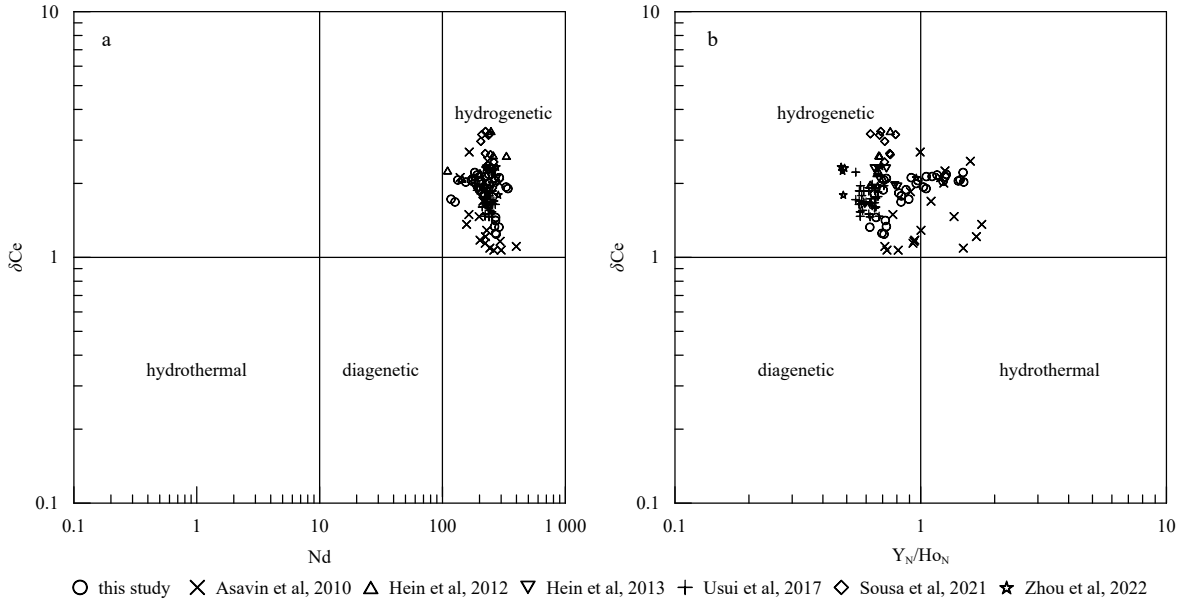

Fig. 5. Element correlation diagram in cobalt-rich crusts: a. δCe vs. Nd; b. δCe vs. Y_N/Ho_N. $\delta Ce = 2Ce_N/(La_N + Pr_N)$. La_N, Ce_N, Pr_N, Y_N and Ho_N are normalized by NASC, and NASC data are from Wang et al. (1989).

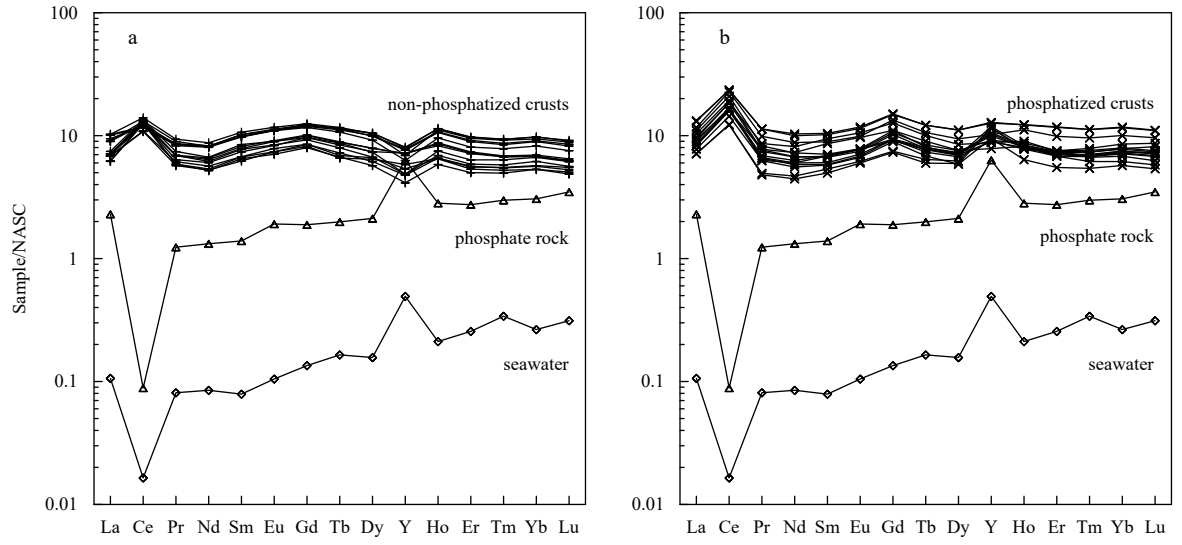

Fig. 6. NASC-normalized REE distribution patterns for cobalt-rich crusts: NASC and seawater data are from Wang et al (1989), non-phosphatized crusts, phosphatized crusts and phosphate rock data are from this study.

Ni are mainly enriched in the Mn oxide phase, and Fe, P, Ti, Cu, Pb, V, Zn, Zr, Mo and REEs are mainly enriched in the Fe oxide phase, and Al and K are mainly enriched in the residual phase. Thus, about 67% of REEs are enriched in the Fe oxide phase, and about 17% in the Mn oxide phase, and only about 13% in the residual phase, and yet the contents of these elements in carbonate phase is relatively small. In contrast, in the phosphatized crusts XD3(Ⅳ) and XD3(Ⅴ), the distribution ratios of Ca, P and REEs in the residual phase increase, and the proportion ratios of REEs increase from 13% to 64%, Ca from 0.54% to 55%, and P from 11% to 40%. Therefore, in the phosphatized crusts, about 64% of REEs are enriched in the residual phase containing carbonate fluorapatite, but the influence of Fe and Mn oxide phases is greatly reduced, which is consistent with the results of Koschinsky et al. (Koschinsky and Hein, 2003; Koschinsky et al., 2020).

The cobalt-rich crusts are hydrogenetic, and the elements mainly come from seawater (Hein et al., 2016; Halbach et al., 2017). According to the results of mineral identification, the carbonate phase is mainly composed of calcite and other minerals, and Na, K, Ca, Mg and Sr in seawater mainly exist in the form of free cations and then enter the carbonate phase (together with carbonate minerals) through ion exchange or adsorption (Koschinsky and Hein, 2003; Bai et al., 2004). The Mn oxide phase is mainly composed of vernadite (δ-MnO_2), and Ba, Sr, Co and Ni in seawater are enriched in the Mn oxide phase by adsorption during the formation of Mn colloidal particles (He et al., 2005, 2011). The Fe oxide phase is mainly composed of amorphous ferric oxyhydroxide (FeOOH), and P, Ti, Cu, Pb, V, Zn, Zr and REEs in seawater are enriched in the Fe oxide phase by adsorption during the formation of Fe colloidal particles (Koschinsky and Hein, 2003; Koschinsky et al., 2020). The residual phase is mainly composed of quartz, feldspar and other minerals, containing silicon aluminate such as Si, Al and K, which are mainly derived from terrigenous detrital materials and enriched in cobalt-rich crusts

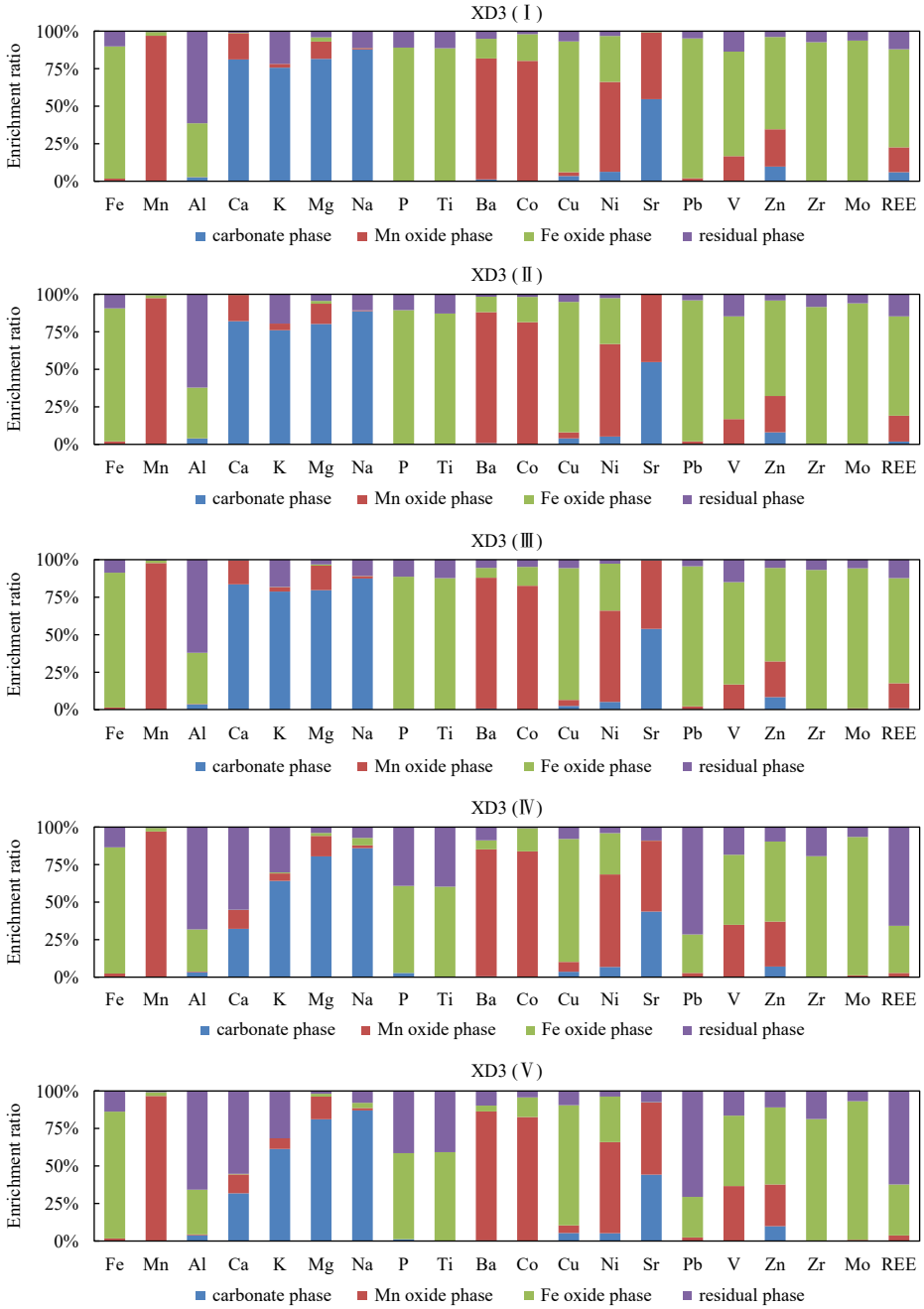

Fig. 7. The occurrence phase of elements in structural layers of cobalt-rich crusts.

by seawater exchange (Hein et al., 2016).

Multiple phosphatization events occur during the early growth of cobalt-rich crusts (Koschinsky et al., 1997; Hein et al., 2000). Due to the effect of phosphatization, Ca and P contents in the old crusts are generally high, and there are CFA minerals (Ren et al., 2017). During the growth of carbonate fluorapatite, some elements have undergone secondary enrichment, and REEs are transferred and enriched in the phosphate phase. Due to the similar radius of REE^{3+} and Ca^{2+}, REE^{3+} can effectively combine with PO_4^{3-} instead of Ca^{2+} and form rare earth phosphate minerals (Koschinsky et al., 2020). In contrast, REE contents of phosphate selected from the crusts are much lower than those of the crusts, indicating that REE contents of phosphate in the crusts are not uniform, the rich rare earth phosphate is difficult to separate from the crusts. Consequently, the simulation results of the mixture of crusts and phosphates showed that (Ren et al., 2017), there should be rich rare earth phosphate in the phosphatized crusts, which may be disseminated in the crusts, representing a relatively slow phosphate precipitation process. The results of the cobalt-rich crusts from Magellan Seamounts showed that (Ren et al., 2011a), up to 42%–88% of REEs in the phosphatized crusts are contributed from phosphate, and it is inferred that there may be independent rare earth phosphate minerals. Therefore, further research is needed on the combination of rare earth elements with phosphate to form rare earth phosphate minerals.

4.3 *Influencing factors of REE enrichment*

The variation curves of element contents with depth in the growth profile of cobalt-rich crust sample XD3 are shown in Fig. 8. The results show that, REE contents increase from the new crusts to the old crusts, and there is a highest value in the old

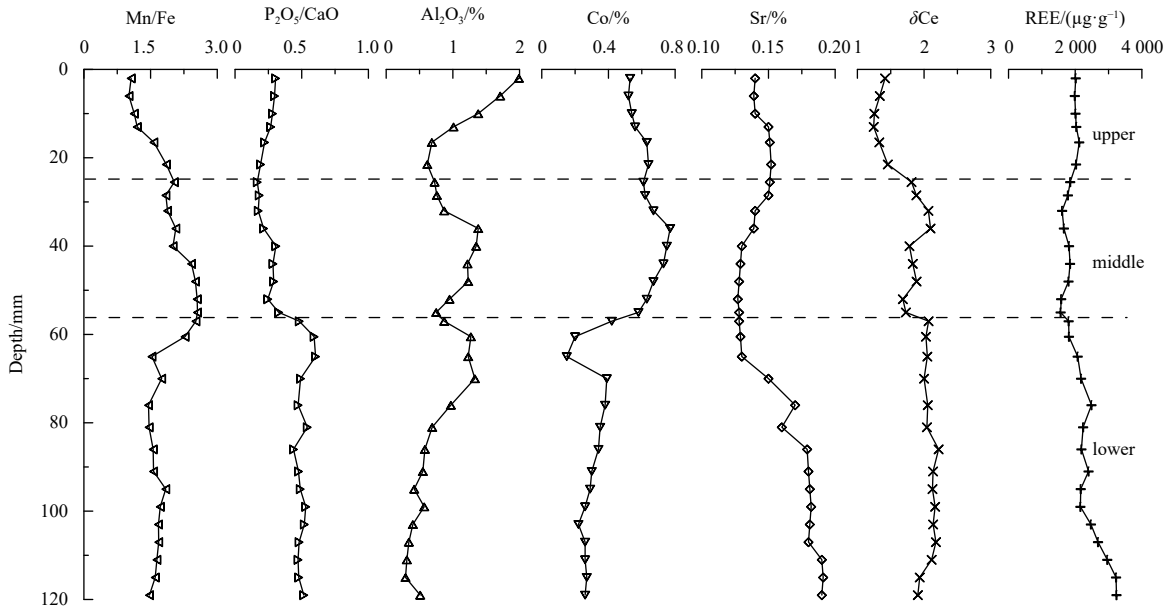

Fig. 8. Variation curves of element contents with depth in the growth profile of cobalt-rich crusts.

crusts. When CaO/P_2O_5 ratio is less than 2, it indicates that the cobalt-rich crusts have a phosphatization event (Koschinsky et al., 1997; Ren et al., 2016). In the study, CaO/P_2O_5 ratio of the old crusts ranges from 1.66 to 2.28, indicating that the phosphatization occurs in the old crusts. The P_2O_5/CaO ratio does not change much in the new crusts, but increases in the old crusts, and REE contents also increase, which indicates that phosphatization can promote the REE enrichment. When Mn/Fe ratio is less than 2.5, it indicates that the cobalt-rich crusts are hydrogenetic (Halbach et al., 1983; Hou et al., 2020). In the study, Mn/Fe ratio ranges from 1.01 to 2.56, indicating that the cobalt-rich crusts are hydrogenetic and REEs mainly come from seawater. Moreover, the δCe can indicate the redox environment of seawater during forming cobalt-rich crusts (Hein et al., 2000). During the growth period of the old crusts, δCe is higher, seawater is an oxidizing environment, and REE contents are higher relative to the new crusts, which indicates that the oxidizing environment of seawater can promote the REE enrichment. The variations of Sr contents can be used to indicate the degree of marine productivity (Li et al., 2011). During the growth period of the old crusts, Sr content is higher, marine productivity is higher, and REE contents are higher relative to the new crusts, which indicates that high marine productivity can promote the REE enrichment. Meanwhile, the variations of Co contents can indicate the growth rate of cobalt-rich crusts (Ren et al., 2011b). During the growth period of the old crusts, Co content is lower, the growth rate is slower, and REE contents are higher relative to the new crusts, which indicates that the slow growth rate can promote the REE enrichment. The variations of Al_2O_3 can indicate the sedimentation of terrigenous detrital materials (Cui et al., 2012). During the growth period of the new crusts, Al content is higher, terrigenous detrital materials are more, and REE contents are lower relative to the old crusts, which indicates that terrigenous detrital materials can dilute REE when they enter cobalt-rich crusts. As above mentioned, the variation of REEs is similar to that of P_2O_5/CaO, Mn/Fe, δCe and Sr, indicating that the oxidizing environment of seawater, high marine productivity, phosphatization, and slow growth rate can promote the REE enrichment.

5 Conclusions

This study analyzes the mineral composition and REE contents of cobalt-rich crusts from Marcus-Wake Seamounts in the Pacific, and discuss the source, occurrence phases and enrichment mechanism of REEs.

(1) The major crystalline mineral of cobalt-rich crusts from Marcus-Wake Seamounts is vernadite, and the secondary minerals include quartz, plagioclase and carbonate fluorapatite. Also many amorphous ferric oxyhydroxides are contained in cobalt-rich crusts.

(2) Mn and Fe contents are higher relative to other elements, and REE are enriched in the cobalt-rich crusts. REE contents of the old crusts are higher than those of the new crusts. The non-phosphatized crusts have positive Ce and negative Y anomalies, and yet the phosphatized crusts have positive Ce and positive Y anomalies, indicating that cobalt-rich crusts are hydrogenetic, and REE mainly come from seawater.

(3) The occurrence phases of elements are closely related to their mineral phases. In the non-phosphatized crusts, REEs are adsorbed by colloidal particles into the crusts, about 67% of REEs are enriched in the Fe oxide phase. In contrast, the phosphatized crusts are affected by the phosphatization, REEs may combine with phosphate to form rare earth phosphate minerals, and about 64% of REEs are enriched in the residual phase containing carbonate fluorapatite.

(4) The variation of REEs is similar to that of P_2O_5/CaO, Mn/Fe, δCe and Sr, indicating that the oxidizing environment of seawater, high marine productivity, phosphatization, and slow growth rate can promote the REE enrichment.

References

Asavin A M, Kubrakova I V, Mel'nikov M E, et al. 2010. Geochemical zoning in ferromanganese crusts of Ita-MaiTai Guyot. Geochemistry International, 48(5): 423–445, doi: 10.1134/S0016702910050010

Azami K, Hirano N, Machida S, et al. 2018. Rare earth elements and yttrium (REY) variability with water depth in hydrogenetic ferromanganese crusts. Chemical Geology, 493: 224–233, doi: 10.1016/j.chemgeo.2018.05.045

Bai Zhimin, Wang Yingbin, Jiang Bo, et al. 2004. Occurrence modes

of REE in the Pacific cobalt-rich crusts. Earth Science Frontiers (in Chinese), 11(2): 387–392

Bau M, Koschinsky A. 2009. Oxidative scavenging of cerium on hydrous Fe oxide: evidence from the distribution of rare earth elements and yttrium between Fe oxides and Mn oxides in hydrogenetic ferromanganese crusts. Geochemical Journal, 43(1): 37–47, doi: 10.2343/geochemj.1.0005

Bau M, Schmidt K, Koschinsky A, et al. 2014. Discriminating between different genetic types of marine ferro-manganese crusts and nodules based on rare earth elements and yttrium. Chemical Geology, 381: 1–9, doi: 10.1016/j.chemgeo.2014.05.004

Bonatti E, Kraemer T, Rydell H. 1972. Classification and genesis of submarine iron-manganese deposits. In: Horn D R, ed. Ferromanganese Deposits of the Ocean Floor. Washington, US: National Science Foundation, 149–166

Charles C, Pelleter E, Révillon S, et al. 2020. Intermediate and deep ocean current circulation in the Mozambique Channel: new insights from ferromanganese crust Nd isotopes. Marine Geology, 430: 106356, doi: 10.1016/j.margeo.2020.106356

Conrad T, Hein J R, Paytan A, et al. 2017. Formation of Fe-Mn crusts within a continental margin environment. Ore Geology Reviews, 87: 25–40, doi: 10.1016/j.oregeorev.2016.09.010

Cui Yingchun, Shi Xuefa, Liu Jihua, et al. 2012. Records of past 70 Ma dust activities in ferromanganese crusts from Pacific Ocean. Journal of Jilin University (Earth Science Edition) (in Chinese), 42(2): 393–399

Fukami Y, Kashiwabara T, Amakawa H, et al. 2022. Tellurium stable isotope composition in the surface layer of ferromanganese crusts from two seamounts in the Northwest Pacific Ocean. Geochimica et Cosmochimica Acta, 318: 279–291, doi: 10.1016/j.gca.2021.12.005

Gao Jingjing, Liu Jihua, Li Xianguo, et al. 2015. Chemical phase analysis of rare earth elements in cobalt-rich crusts and its application. Chinese Journal of Analytical Chemistry (in Chinese), 43(12): 1895–1900

Gao Jingjing, Liu Jihua, Zhang Hui, et al. 2023. Geochemistry and occurrence phase of the elements in cobalt-rich crusts from the Magellan Seamounts. Oceanologia et Limnologia Sinica (in Chinese), 54(2): 424–435

Goto K T, Nozaki T, Toyofuku T, et al. 2017. Paleoceanographic conditions on the São Paulo Ridge, SW Atlantic Ocean, for the past 30 million years inferred from Os and Pb isotopes of a hydrogenous ferromanganese crust. Deep-Sea Research Part II: Topical Studies in Oceanography, 146: 82–92, doi: 10.1016/j.dsr2.2016.10.010

Gueguen B, Rouxel O, Fouquet Y. 2021. Nickel isotopes and rare earth elements systematics in marine hydrogenetic and hydrothermal ferromanganese deposits. Chemical Geology, 560: 119999, doi: 10.1016/j.chemgeo.2020.119999

Gueguen B, Rouxel O, Rouget M L, et al. 2016. Comparative geochemistry of four ferromanganese crusts from the Pacific Ocean and significance for the use of Ni isotopes as paleoceanographic tracers. Geochimica et Cosmochimica Acta, 189: 214–235, doi: 10.1016/j.gca.2016.06.005

Halbach P. 1986. Processes controlling the heavy metal distribution in Pacific ferromanganese nodules and crusts. Geologische Rundschau, 75(1): 235–247, doi: 10.1007/BF01770191

Halbach P, Segl M, Puteanus D, et al. 1983. Co-fluxes and growth rates in ferromanganese deposits from central Pacific seamount area. Nature, 304(5928): 716–719, doi: 10.1038/304716a0

Halbach P E, Jahn A, Cherkashov G. 2017. Marine Co-rich ferromanganese crust deposits: description and formation, occurrences and distribution, estimated world-wide resources. In: Sharma R, ed. Deep-Sea Mining: Resource Potential, Technical and Environmental Considerations. Cham: Springer International Publishing, 65–141

He Gaowen, Sun Xiaoming, Yang Shengxiong, et al. 2011. A comparison of REE geochemistry between polymetallic nodules and cobaltrich crusts in the Pacific Ocean. Geology in China (in Chinese), 38(2): 462–472

He Gaowen, Xue Ting, Sun Xiaoming, et al. 2005. The Elemental association characterisitics and the geological significance of cobalt-rich crusts in the West Pacific Ocean. Bulletin of Mineralogy, Petrology and Geochemistry (in Chinese), 24(2): 125–129

Hein J R, Conrad T A, Frank M, et al. 2012. Copper-nickel-rich, amalgamated ferromanganese crust-nodule deposits from Shatsky Rise, NW Pacific. Geochemistry, Geophysics, Geosystems, 13(10): Q10022

Hein J R, Conrad T, Mizell K, et al. 2016. Controls on ferromanganese crust composition and reconnaissance resource potential, Ninetyeast Ridge, Indian Ocean. Deep-Sea Research Part I: Oceanographic Research Papers, 110: 1–19, doi: 10.1016/j.dsr.2015.11.006

Hein J R, Koschinsky A. 2014. Deep-ocean ferromanganese crusts and nodules. In: Holland H D, Turekian K K, eds. Treatise on Geochemistry. 2nd ed. Oxford: Elsevier Limited, 273–291

Hein J R, Koschinsk A, Bau M, et al. 2000. Cobalt-rich ferromanganese crusts in the Pacific. In: Cronan D S, ed. Handbook of Marine Mineral Deposits. Boca Raton, Florida: CRC Press, 239–279

Hein J R, Mizell K, Koschinsky A, et al. 2013. Deep-ocean mineral deposits as a source of critical metals for high- and green-technology applications: comparison with land-based resources. Ore Geology Reviews, 51: 1–14, doi: 10.1016/j.oregeorev.2012.12.001

Hou Xiaofan, Wang Zhenyan, Li Wenjian, et al. 2020. Mineralogy and geochemistry of ferromanganese crusts of Caroline ridge CM4 guyot in the western Pacific. Oceanologia et Limnologia Sinica (in Chinese), 51(5): 1118–1126

Huang Wei, Hu Bangqi, Song Weiyu, et al. 2022. Enrichment and constraints of critical metals in ferromanganese crusts from 13°20'N seamount of the southern Kyushu-Palau Ridge. Marine Geology & Quaternary Geology (in Chinese), 42(5): 137–148.

Jiang Xiaodong, Sun Xiaoming, Chou Yumin, et al. 2020. Geochemistry and origins of carbonate fluorapatite in seamount Fe-Mn crusts from the Pacific Ocean. Marine Geology, 423: 106135, doi: 10.1016/j.margeo.2020.106135

Josso P, Lusty P, Chenery S, et al. 2021. Controls on metal enrichment in ferromanganese crusts: temporal changes in oceanic metal flux or phosphatisation? Geochimica et Cosmochimica Acta, 308: 60–74

Josso P, Pelleter E, Pourret O, et al. 2017. A new discrimination scheme for oceanic ferromanganese deposits using high field strength and rare earth elements. Ore Geology Reviews, 87: 3–15, doi: 10.1016/j.oregeorev.2016.09.003

Josso P, Parkinson I, Horstwood M, et al. 2019. Improving confidence in ferromanganese crust age models: a composite geochemical approach. Chemical Geology, 513: 108–119, doi: 10.1016/j.chemgeo.2019.03.003

Josso P, Rushton J, Lusty P, et al. 2020. Late Cretaceous and Cenozoic paleoceanography from north-east Atlantic ferromanganese crust microstratigraphy. Marine Geology, 422: 106122, doi: 10.1016/j.margeo.2020.106122

Khanchuk A I, Mikhailik P E, Mikhailik E V, et al. 2015. Peculiarities of the distribution of rare-earth elements and yttrium in mineral phases of the ferromanganese crusts from the Detroit Guyot (Pacific Ocean). Doklady Earth Sciences, 465(2): 1243–1247, doi: 10.1134/S1028334X15120016

Konstantinova N, Hein J R, Mizell K, et al. 2020. Changes in sediment source areas to the Amerasia Basin, Arctic Ocean, over the past 5.5 million years based on radiogenic isotopes (Sr, Nd, Pb) of detritus from ferromanganese crusts. Marine Geology, 428: 106280, doi: 10.1016/j.margeo.2020.106280

Konstantinova N, Son V T, Thang L A, et al. 2022. Ferromanganese crusts of the Vietnam margin, central South China Sea: composition and genesis. Marine Geology, 453: 106911, doi: 10.1016/j.margeo.2022.106911

Koschinsky A, Halbach P. 1995. Sequential leaching of marine ferromanganese precipitates: genetic implications. Geochimica et Cosmochimica Acta, 59(24): 5113–5132, doi: 10.1016/0016-7037(95)00358-4

Koschinsky A, Hein J R. 2003. Uptake of elements from seawater by ferromanganese crusts: solid-phase associations and seawater speciation. Marine Geology, 198(3-4): 331–351, doi: 10.1016/S0025-3227(03)00122-1

Koschinsky A, Hein J R, Kraemer D, et al. 2020. Platinum enrichment and phase associations in marine ferromanganese crusts and nodules based on a multi-method approach. Chemical Geology, 539: 119426, doi: 10.1016/j.chemgeo.2019.119426

Koschinsky A, Stascheit A, Bau M, et al. 1997. Effects of phosphatization on the geochemical and mineralogical composition of marine ferromanganese crusts. Geochimica et Cosmochimica Acta, 61(19): 4079–4094, doi: 10.1016/S0016-7037(97)00231-7

Li Jiangshan, Shi Xuefa, Liu Jihua, et al. 2011. Constraints of paleoceanographic environmental evolution on REEs enrichment in Co-rich crust. Journal of the Chinese Society of Rare Earths (in Chinese), 29(5): 622–629

Liu Kai, Wang Zhenyan. 2021. Geochemistry of rare earth elements and yttrium in ferromanganese crusts from Kocebu Guyot in the Western Pacific. Marine Geology & Quaternary Geology (in Chinese), 41(1): 210–222

Lusty P A J, Hein J R, Josso P. 2018. Formation and occurrence of ferromanganese crusts: earth's storehouse for critical metals. Elements, 14(5): 313–318, doi: 10.2138/gselements.14.5.313

Marino E, González F J, Kuhn T, et al. 2019. Hydrogenetic, diagenetic and hydrothermal processes forming ferromanganese crusts in the Canary Island Seamounts and their influence in the metal recovery rate with hydrometallurgical methods. Minerals, 9(7): 439, doi: 10.3390/min9070439

Marino E, González F J, Somoza L, et al. 2017. Strategic and rare elements in Cretaceous-Cenozoic cobalt-rich ferromanganese crusts from seamounts in the Canary Island Seamount Province (northeastern tropical Atlantic). Ore Geology Reviews, 87: 41–61, doi: 10.1016/j.oregeorev.2016.10.005

Mikhailik P E, Mikhailik E V, Zarubina N V, et al. 2017. Distribution of rare-earth elements and yttrium in hydrothermal sedimentary ferromanganese crusts of the Sea of Japan (*from phase analysis results*). Russian Geology and Geophysics, 58(12): 1530–1542, doi: 10.1016/j.rgg.2017.11.013

Mohwinkel D, Kleint C, Koschinsky A. 2014. Phase associations and potential selective extraction methods for selected high-tech metals from ferromanganese nodules and crusts with siderophores. Applied Geochemistry, 43: 13–21, doi: 10.1016/j.apgeochem.2014.01.010

Nath B N, Roelandts I, Sudhakar M, et al. 1994. Cerium anomaly variations in ferro-manganese nodules and crusts from the Indian Ocean. Marine Geology, 120(3-4): 385–400, doi: 10.1016/0025-3227(94)90069-8

Nishi K, Usui A, Nakasato Y, et al. 2017. Formation age of the dual structure and environmental change recorded in hydrogenetic ferromanganese crusts from Northwest and Central Pacific seamounts. Ore Geology Reviews, 87: 62–70, doi: 10.1016/j.oregeorev.2016.09.004

Pan Jiahua, De Carlo E H, Yang Yi, et al. 2005. Effect of phosphatization on element concentration of cobalt-rich ferromanganese crusts. Acta Geoscientia Sinica (English Edition), 79(3): 349–355, doi: 10.1111/j.1755-6724.2005.tb00900.x

Pan Jiahua, Liu Shuqin, DeCarlo E. 2002. The effects of marine phospharization on element concentration of cobalt-rich crusts. Acta Geoscientia Sinica (in Chinese), 23(5): 403–407

Pelleter E, Fouquet Y, Etoubleau J, et al. 2017. Ni-Cu-Co-rich hydrothermal manganese mineralization in the Wallis and Futuna back-arc environment (SW Pacific). Ore Geology Reviews, 87: 126–146, doi: 10.1016/j.oregeorev.2016.09.014

Ren Jiangbo, He Gaowen, Yao Huiqiang, et al. 2016. Geochemistry and significance of REE and PGE of the cobalt-rich crusts from west Pacific Ocean seamounts. Earth Science (in Chinese), 41(10): 1745–1757

Ren Jiangbo, He Gaowen, Yao Huiqiang, et al. 2017. The effects of phosphatization on the REY of Co-rich Fe-Mn crusts. Marine Geology & Quaternary Geology (in Chinese), 37(2): 33–43

Ren Xiangwen, Liu Jihua, Shi Xuefa, et al. 2011b. Genesis and ore-forming stages of Co-rich ferromanganese crusts from Seamount M of Magellan Seamounts: evidence from geochemistry and Co chronology. Marine Geology & Quaternary Geology (in Chinese), 31(6): 65–74

Ren Xiangwen, Shi Xuefa, Zhu Aimei, et al. 2011a. Existing phase of rare earth elements in Co-rich Fe-Mn crusts from seamount MK of Magellan seamount cluster. Journal of Jilin University (Earth Science Edition) (in Chinese), 41(3): 707–714

Sousa I M C, Santos R V, Koschinsky A, et al. 2021. Mineralogy and chemical composition of ferromanganese crusts from the Cruzeiro do Sul Lineament-Rio Grande Rise, South Atlantic. Journal of South American Earth Sciences, 108: 103207, doi: 10.1016/j.jsames.2021.103207

Surya P L, Durbar R, Nagender N B, et al. 2020. Anomalous phase association of REE in ferromanganese crusts from Indian mid-oceanic ridges: evidence for large scale dispersion of hydrothermal iron. Chemical Geology, 549: 119679, doi: 10.1016/j.chemgeo.2020.119679

Usui A, Nishi K, Sato H, et al. 2017. Continuous growth of hydrogenetic ferromanganese crusts since 17 Myr ago on Takuyo-Daigo Seamount, NW Pacific, at water depths of 800–5500 m. Ore Geology Reviews, 87: 71–87, doi: 10.1016/j.oregeorev.2016.09.032

Wang Zhonggang, Yu Xueyuan, Zhao Zhenhua, et al. 1989. Rare Earth Elements Geochemistry (in Chinese). Beijing: Science Press, 1–535

Xu Zhaokai, Li Anchun, Yu Xinke, et al. 2008. Elemental occurrence Phases of the new-type ferromanganese crusts from the East Philippine Sea. Earth Science-Journal of China University of Geosciences (in Chinese), 33(3): 329–336, doi: 10.3799/dqkx.2008.043

Zhong Yi, Chen Zhong, González F J, et al. 2017. Composition and genesis of ferromanganese deposits from the northern South China Sea. Journal of Asian Earth Sciences, 138: 110–128, doi: 10.1016/j.jseaes.2017.02.015

Zhou Jiao, Cai Pengjie, Yang Chupeng, et al. 2022. Geochemical characteristics and genesis of ferromanganese nodules and crusts from the Central Rift Seamounts Group of the West Philippine Sea. Ore Geology Reviews, 145: 104923, doi: 10.1016/j.oregeorev.2022.104923